Pyroelectric properties of polydomain epitaxial Pb(Zr_{1-x},Ti_{x})O_{3} thin films

J. Karthik and L. W. Martin

Phys. Rev. B **84**, 024102 — Published 1 July 2011

DOI: 10.1103/PhysRevB.84.024102

Pyroelectric properties of polydomain epitaxial $Pb(Zr_{1-x},Ti_x)O_3$ thin films

J. Karthik and L. W. Martin*

Department of Materials Science and Engineering and Frederick Seitz Materials Research Laboratory, University of Illinois, Urbana-Champaign, Urbana, IL 61801

*lwmartin@illinois.edu

Abstract

The pyroelectric properties of polydomain epitaxial $Pb(Zr_{1-x},Ti_x)O_3$ thin films are investigated using a Ginzburg-Landau-Devonshire thermodynamic model. We explore the three major contributions to pyroelectric response in thin films including intrinsic effects and previously neglected contributions such as extrinsic and secondary effects, to provide a complete picture of pyroelectric property development. The pyroelectric coefficient for epitaxial thin films is calculated as a function of strain, temperature, and composition for $0.5 \leq x \leq 1.0$. We find that structural transitions driven by epitaxial strain can greatly enhance the pyroelectric coefficient and that extrinsic contributions due to temperature driven domain wall motion can significantly alter the intrinsic pyroelectric properties. Furthermore, we show that the pyroelectric coefficient at room temperature is maximized at the multicritical point between various polydomain phases and is also consistently high along the boundary between the *c/ a/ c/ a* and a_1 / a_2 / a_1 / a_2 polydomain phases. Additionally, we have investigated the impact of epitaxial strain on pyroelectric response in polydomain states and found that the extrinsic contribution from domain walls to the pyroelectric coefficient varies depending on the sign of the strain. Finally we examine the addition of secondary contributions to pyroelectricity that arise from thermal expansion in materials and provide insight into the effect of this contribution on the overall magnitude of response.

I. INTRODUCTION

Ferroelectric materials such as $Pb(Zr_{1-x},Ti_x)O_3$ (PZT) and $(Ba_{1-x}Sr_x)TiO_3$ (BST) have been a subject of intense theoretical and experimental study due to their robust and tunable ferroelectric properties that enable a wide variety of applications. In general, these materials possess a rich composition dependent phase diagram and the dielectric, piezoelectric, and pyroelectric properties of these materials can be adjusted with composition to suit a given application.[1] Modern applications of ferroelectric materials increasingly call for the use of thin films that enable microfabricated devices on a variety of different substrates.[2,3,4] In thin films, the properties of these materials can also be engineered with epitaxial strain,[4] thickness,[5] electrical boundary conditions,[6] and more. Recent work on strain engineering of ferroelectrics, for instance, has demonstrated spectacular results including strain induced ferroelectricity in $SrTiO_3$,[7] rotational phases in ultrathin $PbTiO_3$,[8] and strain driven morphotropic phase boundary-like features in $BiFeO_3$.[9] Thus epitaxial strain has become one of the most powerful tools for enhancing and controlling the properties in complex oxide systems and a route to harnessing phenomena that may be absent in bulk materials. Among the many useful properties of ferroelectrics, pyroelectricity has been the focus of detailed study.[10,11] The pyroelectric effect describes the process by which materials generate a temporary electrical potential when heated or cooled. This effect arises from temperature-dependent changes in the spontaneous polarization (P_s) that result in the flow of charge to and from the surface of the ferroelectric.[12]

Ferroelectric thin films have been used in a wide range of pyroelectric applications ranging from thermal imaging to laser detection[13] and recent developments in the energy landscape are poised to call these materials into service for energy applications with increasing frequency. One possibility is to use these materials to harvest waste heat for energy production

through a process called pyroelectric energy harvesting.[14] Materials having a large pyroelectric coefficient should have the capacity for high efficiency pyroelectric energy conversion.[15] Ferroelectric and relaxor materials with high dielectric constants are excellent candidates for energy conversion as they have high polarization and can store high densities of electrical energy. Recent studies include attempts at energy conversion using bulk crystals of relaxor materials[15] and ferroelectric nanowires.[16]

Since most practical applications utilize "thick" ferroelectric films (generally in excess of 200 nm), it is important to understand pyroelectricity in these systems and explore new mechanisms for improving the pyroelectric coefficient. Epitaxial ferroelectric thin films which possess ferroelectric properties that are tunable with strain, composition, and temperature offer an exciting potential for such a study, but a comprehensive theoretical understanding is currently unavailable. Pyroelectric properties of ferroelectric thin films have been calculated using Ginzburg-Landau-Devonshire (GLD) theories previously,[17,18] but most have concentrated on monodomain films at a few chosen compositions. It is known, however, that monodomain states are stable only in ultrathin films of PZT[19,20] and thicker films, that are more technologically relevant, form polydomain states in equilibrium.[21,22,25] GLD theory has been modified to accurately predict the formation and properties of these polydomain states in strained films.[23,24] In this paper, we use a GLD phenomenological model to study pyroelectricity in polydomain structures that form in thick films of the technologically relevant PZT system. We develop a design algorithm that will allow researchers to maximize the pyroelectric coefficient in epitaxial thin films as a function of composition, temperature, and thin film strain. Apart from the intrinsic pyroelectric coefficient due to a temperature dependent change in the polarization in the bulk of the domains, we calculate an extrinsic contribution (or a domain wall contribution) to the

pyroelectric response due the temperature dependent movement of the domain walls in the polydomain states and also explore a secondary effect that arises from a piezoelectric contribution that results from thermal expansion. We observe that this extrinsic contribution, which has been neglected in earlier calculations, can significantly impact the pyroelectric properties of thin films and may offer new pathways to increase pyroelectric coefficient in these systems. The secondary contribution is dependent on the choice of substrate and represents a finer-level adjustment of the models.

II. THERMODYNAMIC ANALYSIS

In this study, we consider the case of single-crystalline epitaxial thin films of a ferroelectric grown in the cubic paraelectric state on a much thicker substrate. During cooling from the growth temperature (T_g) the paraelectric to ferroelectric transition takes place resulting in the formation of a mono or polydomain ferroelectric state at lower temperatures. The monodomain states consists of homogeneous polarization and strains throughout the film while the polydomain state consists of two alternating domains with different polarization states separated by planar domain walls. To identify the equilibrium state of the polydomain films we use the thermodynamic theory of ferroelectric thin films with dense domain structures as developed in Refs. 23 and 24. We assume that the polarization and strain fields inside the individual domains are homogeneous and the domain wall self-energies are negligible. Such an assumption is justified for thick (> 200 nm) PZT films where the theoretically predicted domain structures have been observed experimentally[21,25] and the condition that the domain wall width is much less than the film thickness is satisfied so that the domain wall self-energy may be neglected.[26,27]

We use the generalized Helmholtz free energy density ($\tilde{F}$) for a ferroelectric thin film to obtain the equilibrium pyroelectric properties. In the crystallographic reference frame (x_1, x_2, x_3) of the paraelectric phase $\tilde{F}$ can written in terms of the polarization P_i and stresses σ_i as[23]

$$\begin{aligned}\widetilde{F} = {} & \alpha_1\left(P_1^2+P_2^2+P_3^2\right)+\alpha_{11}\left(P_1^4+P_2^4+P_3^4\right)+\alpha_{12}\left(P_1^2P_2^2+P_2^2P_3^2+P_1^2P_3^2\right)+\alpha_{111}\left(P_1^6+P_2^6+P_3^6\right)+ \\ & \alpha_{112}\left\{P_1^4\left(P_2^2+P_3^2\right)+P_2^4\left(P_3^2+P_1^2\right)+P_3^4\left(P_1^2+P_2^2\right)\right\}+\alpha_{123}P_1^2P_2^2P_3^2+\tfrac{1}{2}s_{11}\left(\sigma_1^2+\sigma_2^2+\sigma_3^2\right)+ \\ & s_{12}\left(\sigma_1\sigma_2+\sigma_2\sigma_3+\sigma_1\sigma_3\right)+\tfrac{1}{2}s_{44}\left(\sigma_4^2+\sigma_5^2+\sigma_6^2\right)-\tfrac{1}{2}\varepsilon_0\left(E_1^2+E_2^2+E_3^2\right)-E_1P_1-E_2P_2-E_3P_3\end{aligned} \quad (1)$$

where P_i are the polarization components. The primary stiffness coefficient (α_1) is given by the 2are the mechanical stresses, s_{ij} are the elements of the elastic compliance tensor at constant polarization, E_i are the components of the internal electric field, C is the Curie constant, and T_c is the ferroelectric Curie temperature. The phenomenological coefficients for the PZT system were obtained from Refs. 28 and 29. The stresses σ_i are related to the polarization components and lattice strains through the electrostrictive coefficients as shown in the equations of state below. Thus, $\tilde{F}$ takes the coupling between the strain and polarization into full account and the transformation of $\tilde{F}$ into a function of P_i and strains S_i restores these coupling terms. The free energy neglects the energies associated with the tilting of the oxygen octahedra and the anti-ferroelectric polarization states. These are valid assumptions for $x \geq 0.5$ and T $\geq$ 300 K which are considered in this paper.[30] For the thick films considered here, we can also neglect the depolarization field due the finite conductivity of the PZT thin films.[31]

The free energy is supplemented by the relevant mechanical boundary conditions for the mono/polydomain structures.[23,30] For the monodomain ferroelectric states, the mechanical boundary conditions give the in-plane strain components as

$$S_1 = S_2 = S_m,\ S_6 = 0$$

where the misfit strain $S_m = \frac{a_s - a_0}{a_0}$ is defined by the substrate lattice parameter a_s and the lattice constant a_0 of the free standing film. Since there are no forces acting on the free surface of the film, we also have $\sigma_3 = \sigma_4 = \sigma_5 = 0$. The remaining three strains (S_3, S_4, and S_5) depend on the polarization P_i in the film through $S_n = -\frac{\partial \tilde{F}}{\partial \sigma_n}$. In the absence of an external electric field, for the case of short-circuited PZT films, we set $E_i = 0$ along all three directions. This enables the description of the free energy of the monodomain states in terms of the polarizations P_i and the epitaxial strain S_m. Minimizing the free energy gives the equilibrium polarization as a function of strain, composition and temperature. For (001) oriented films, the out-of-plane primary pyroelectric coefficient is defined as $\pi_3 = \frac{dP_3}{dT}$ and can be calculated using analytical expressions that relate it to equilibrium polarizations and GLD coefficients.

For the polydomain states, the average free energy density $\langle \tilde{F} \rangle$ can be written as $\langle \tilde{F} \rangle = \phi' F' + (1 - \phi') F''$ where ϕ' is the domain fraction of the first domain type and F' and F'' are the energy densities within the domains of first and second type, respectively. Using mechanical boundary conditions it is possible to eliminate the stresses σ_i', σ_i'' from the expression of $\langle \tilde{F} \rangle$ similar to the single domain case. From the epitaxial relationship determined by the substrate we can express the mean in-plane strains as

$$\langle S_1 \rangle = \langle S_2 \rangle = S_m, \langle S_6 \rangle = 0.$$

The absence of forces acting on the free surfaces implies

$$\langle \sigma_3 \rangle = \langle \sigma_4 \rangle = \langle \sigma_5 \rangle = 0.$$

The strain components inside each domain are related to the free energy as $S_n = -\frac{\delta F}{\delta \sigma_n}$. In polydomain films, these must be supplemented by the microscopic boundary conditions on the domain walls. In the reference frame (x_1', x_2', x_3') with x_3' perpendicular to the domain walls, the strain compatibility in the neighboring domains implies $S_i^t = S_i^{tt}$ $(i = 1, 2, 6)$ and the mechanical equilibrium of the domains implies that the stress components are related as $\sigma_i^t = \sigma_i^{tt}$ $(i = 3, 4, 5)$. Also, the local internal fields E_i^t in a polydomain film are not necessarily equal to the externally applied field. In the absence of depolarizing fields, however, we can set the average electric field $\langle E_i \rangle$ to zero along all 3 directions in the case of short-circuited ferroelectric films considered here. The microscopic electric field continuity equations yield

$$E_1^t = E_1^{tt}, \qquad E_2^t = E_2^{tt}, \qquad \text{and} \qquad \varepsilon_0 E_3^t + P_3^t = \varepsilon_0 E_3^{tt} + P_3^{tt}.$$

Using these relationships the average free energy density $\langle \tilde{F} \rangle$ can be written as a function of 7 variables P_i^t, P_i^{tt} and ϕ^t. Performing the minimization of $\langle \tilde{F} \rangle$, we can find the equilibrium polarizations and domain populations as a function of epitaxial strain, composition and temperature. The average primary pyroelectric coefficient $\langle \pi_3 \rangle$ can be calculated as $\langle \pi_3 \rangle = \frac{d\langle P_3 \rangle}{dT}$. The average primary pyroelectric coefficient in a polydomain film can thus be expressed in terms of the equilibrium polarizations and the GLD coefficients.

In this study, the free energy of 5 monodomain phases and 6 polydomain phases were evaluated numerically and the state with the minimum free energy was chosen as the equilibrium state. The monodomain states considered were the paraelectric phase $(P_1 = P_2 = P_3 = 0)$, c phase $(P_1 = P_2 = 0, P_3 \neq 0)$, r phase $(P_1 = P_2 \neq 0, P_3 \neq 0)$, ca phase $(P_1 \neq 0\ P_2 = 0, P_3 \neq 0)$, and the aa phase $(P_1 = P_2 \neq 0, P_3 = 0)$. It has already been

shown that these are the only stable monodomain states in PZT thin films.[30] Near zero strain, the monodomain r-phase is replaced by the polydomain *c/a/c/a* phase in thick PZT films for Ti-rich compositions [Fig. 1]. In the *c/a/c/a* phase, we have pseudotetragonal *c*-domains (with polarization along [001]) separated from the pseudotetragonal *a*-domains (with polarization along [100]) by 90° domain walls that are parallel to the {101} planes of the cubic substrate. Similarly, in the positive misfit strain region, the monodomain *aa* phase breaks up into the polydomain $a_1/a_2/a_1/a_2$ phase with a_1 and a_2 domains having the same magnitude of polarization and volume fractions but with polarization along [100] and [010], respectively. The a_1 and a_2 domains are separated by domain walls parallel the {110} planes of the substrate as shown in Fig. 1. The average primary pyroelectric coefficient in a direction normal to the substrate ($\langle \pi_3 \rangle$) is zero for the $a_1/a_2/a_1/a_2$ phase due to a vanishing component of P_3. Near the morphotropic phase boundary, we observe a polydomain version of the monodomain ca phase as *ca*/aa*/ca*/aa** due a P_2 instability in thick films. This polydomain state can be understood as *c/a/c/a* phase with a non-zero P_2 in both the ca^* and aa^* domains and in neighboring domains, the polarization component P_2 has the same magnitude and direction [Fig. 1]. For compositions x < 0.6 and near zero strain, we also observe equilibrium polydomain phases due to a P_3 instability. They are termed $ca_1/ca_2/ca_1/ca_2$ and $r_1/r_2/r_1/r_2$ and these reduce the region of stability of the *c/a/c/a* phase at such compositions. In these domain structures, the in-plane polarization components and domain fractions retain the characteristics of the parent $a_1/a_2/a_1/a_2$ or $aa_1/aa_2/aa_1/aa_2$ phase but they exhibit a non-zero out-of-plane polarization P_3. The polarization component in neighboring domains in these structures is related as $P_3^i = -P_3^{ii}$. The primary pyroelectric coefficient of domain structures arising due to a P_3 instability is zero due a

zero $\langle P_3 \rangle$. Thus, we observe a complex domain stability map as a function of strain, composition and temperature as shown in Fig. 1 and this multi-component phase diagram results in a non-intuitive variation of the pyroelectric coefficient.

III. PYROELECTRIC PROPERTIES OF EPITAXIAL PZT THIN FILMS

The pyroelectric properties of a ferroelectric material under short-circuit conditions (i.e., E = 0) are controlled by three components: intrinsic, extrinsic, and secondary contributions. In general, the total pyroelectric coefficient is the sum of the pyroelectric coefficients at constant strain (intrinsic plus extrinsic, sometimes called the primary pyroelectric effect) and the piezoelectric contribution from thermal expansion (secondary pyroelectric effect). The intrinsic contribution to the pyroelectric response arises from a temperature dependent change in the polarization in the bulk of a ferroelectric domain. The extrinsic contribution (or a domain wall contribution) to the pyroelectric response arises due to the temperature dependent movement of the domain walls in the polydomain states. And, finally, the secondary contribution to the pyroelectric response arises from a piezoelectric contribution that results from thermal expansion. In thin film samples, the secondary contribution is related to the difference in thermal expansion between the film and substrate materials. Since pyroelectric measurements are usually performed at zero external electric fields, we can neglect the contribution of temperature dependent dielectric constant to the pyroelectric coefficient and the effect of leakage. To date, both the extrinsic and secondary contributions have generally been neglected in calculations, but in the current treatment we systematically investigate the impact of all three contributions. We begin by investigating the primary pyroelectric effect, before exploring the secondary pyroelectric effect for specific thin film heterostructures.

Based on classical definitions of the pyroelectric effect,[12] it should be noted that one would expect the pyroelectric coefficient to be maximized near phase transitions, polarization instabilities in a system, and by proximity to the Curie temperature. In the PZT system, in the compositional range of interest ($0.5 \leq x \leq 1.0$), the largest polarization value occurs at $x = 1.0$ ($PbTiO_3$), the lowest T_c occurs at $x = 0.5$, a morphotropic phase boundary occurs near $x = 0.5$, and a slew of polarization transitions occur in thin films as a function of strain as shown in Fig. 1. Thus optimization of the pyroelectric coefficient within this phase space at a specific temperature relies on a careful comparison and investigation of effects in these systems. Using the GLD model we have investigated the primary pyroelectric coefficient (π_3) of PZT as a function of composition (x) and strain at room temperature (300 K) [Fig 2 (a)-(f)]. At large compressive strains the monodomain c phase is the equilibrium phase at all compositions studied and the magnitude of the pyroelectric coefficient is observed to decrease with increasing compressive strain. This can be understood as resulting from an increase in T_c with increasing compressive strain which thereby progressively removes the enhancement that comes with proximity to T_c. As the compressive strain is lowered, at a critical strain this monodomain c-phase forms a polydomain *c/a/c/a* phase. Further variations in the strain result in the *c/a/c/a* phase transforming into either a $a_1/a_2/a_1/a_2$ phase (for x > 0.62) or a *ca*/aa*/ca*/aa** phase (for x < 0.62). Additionally, for x < 0.62, the *ca*/aa*/ca*/aa** phase transforms to the $a_1/a_2/a_1/a_2$ phase through the polydomain r-phase and the $ca_1/ca_2/ca_1/ca_2$ phases [Figs. 2 (a)-(f)].

Among the polydomain phases, we observe that the *c/a/c/a* and *ca*/aa*/ca*/aa** polydomains possess non-zero pyroelectric coefficients along the 3-direction. For these domain structures, the average out-of-plane polarization is $\langle P_3 \rangle = \phi' P_3'$ and the primary pyroelectric

coefficient can be calculated as $\langle \pi_3 \rangle = \phi' \frac{dP_3'}{dT} + P_3' \frac{d\phi'}{dT}$. The first term represents the intrinsic pyroelectric response due to a temperature dependent change in the magnitude of the polarization within the domains. Since the equilibrium domain population ϕ' also depends on temperature, we have an extrinsic contribution to the primary pyroelectric coefficient as shown in the second term. Physically, this term arises due to the rotation of the polarization in the region swept by the domain wall as it moves under the influence of the changing temperature. The thermodynamic theory enables us to quantify this effect and calculate the intrinsic and extrinsic contribution individually. For the *c/a/c/a* phase, the equilibrium domain fraction ϕ' is obtained as[23]

$$\phi' = 1 - \frac{(s_{11} - s_{12})(S_m - Q_{12}P_3^2)}{s_{11}(Q_{11} - Q_{12})P_3^2} \tag{2}$$

Where Q_{ij} are the electrostrictive coefficients and S_m is the misfit strain. Thus, the extrinsic contribution can be calculated using

$$\frac{d\phi'}{dT} = \frac{2(s_{11} - s_{12})S_m}{s_{11}(Q_{11} - Q_{12})P_3^3} \frac{dP_3}{dT} \tag{3}.$$

For the compositions considered here, the sign of the extrinsic contribution for the $c/a/c/a$ phase depends on the sign of $S_m \frac{dP_3}{dT}$ only. Since the intrinsic pyroelectric coefficient $\frac{dP_3}{dT}$ is always negative, the extrinsic pyroelectric coefficient is positive for compressive strains and negative for tensile strains. Therefore, the extrinsic contribution opposes the intrinsic effect for compressive strains and enhances the intrinsic effect for tensile strains in the *c/a/c/a* phase as shown in Figs. 2 (a)-(f) (blue curves represent the intrinsic contribution alone and red curves the combination of intrinsic and extrinsic). Physically, this can be understood as follows: the *c/a/c/a* phase is confined by the c phase (with a larger P_3) in the compressive regime and the $a_1/a_2/a_1/a_2$

phase (with a lower P_3) in the tensile regime; therefore, the fraction of the *c* phase in the polydomain state shows opposing trends with temperature in the tensile and compressive regimes [Fig. 3]. With increasing temperature, the fraction of the *c* phase increases at compressive strains, but decreases at tensile strains. The spontaneous polarization, however, decreases with temperature at both compressive and tensile strains. Thus, at compressive stains, P_s decreases but the fraction ϕ' increases and the two contributions oppose one another. At tensile strains, P_s decreases and the fraction ϕ' also decreases, therefore the two effects support each other. In ferroelectric thin films, the out-of-plane polarization typically increases under compressive strain and decreases under tensile strain[23] so this effect of strain on the extrinsic pyroelectric coefficient in polydoman states is likely to be a general feature in ferroelectric thin films. From Fig. 2, it is clear that this extrinsic effect significantly alters the intrinsic pyroelectric response and, therefore, the pyroelectric coefficient can be significantly enhanced in tensile strained films. This analysis also serves to explain the giant pyroelectric effect observed in thick self-supported $BaTiO_3$ films at a critical elongation between 2-4%.[32] In that case, the authors noted that the large pyroelectric coefficient that was observed could not be attributed to the intrinsic or the dielectric contributions (due to a change in dielectric constant with temperature). It was surmised that the *c* – *a* domain switching mediated by 90° domain walls could be responsible for this observed effect, but no explanation was provided for the presence of a critical tensile strain or the actual mechanism involved. Our theoretical calculations present a mechanism for the observed effect and provide a physical basis for the presence of a critical tensile strain. A quantitative comparison with theory is, however, not possible here since the poled polycrystalline $BaTiO_3$ films were buckled and the exact value of the tensile strain under the electrical contacts (that corresponds to the 2-4% elongation) is difficult to estimate.

Further, in the case of PZT thin films, since the *c/a/c/a* phase persists into the tensile strain only for Ti-rich compositions [Fig. 1], we see that the large pyroelectric coefficients are obtained for Ti-rich films at the boundary between the *c/a/c/a* and $a_1/a_2/a_1/a_2$ phases. At Ti compositions closer to the morphotropic phase boundary [$x < 0.6$], the polydomain *c/a/c/a c/a/c/a* persists only in the compressive regime and the domain wall effects result in a low pyroelectric coefficient. Instead of the *c/a/c/a* phase, near the morphotropic phase boundary, we observe the *ca*/aa*/ca*/aa** phase with a non-zero $\langle \pi_3 \rangle$. For this phase, we can calculate the equilibrium volume fraction as

$$\phi' = \frac{S_m(s_{11}-s_{12}) + (s_{12}Q_{12} - s_{11}Q_{11})P_3^2 + (s_{12}Q_{11} - s_{11}Q_{12})P_2^2}{s_{11}(Q_{12}-Q_{11})P_3^2} \tag{4}$$

And the extrinsic contribution using

$$\frac{d\phi'}{dT} = \frac{2(s_{11}-s_{12})S_m}{s_{11}(Q_{11}-Q_{12})P_3^3}\frac{dP_3}{dT} + \frac{2(s_{12}Q_{11}-s_{11}Q_{12})P_2}{s_{11}(Q_{12}-Q_{11})P_3^3}\left\{P_3\frac{dP_2}{dT} - P_2\frac{dP_3}{dT}\right\} \tag{5}$$

Where P_2, P_3 are polarization components in the *ca** domain.

Upon a complete optimization of the pyroelectric coefficient with strain and composition [Fig. 4] a clear picture begins to emerge. We find that the room temperature (300 K) pyroelectric coefficient is maximum ($\langle \pi_3 \rangle$ = -0.045 μC/cm^{2}K) at a composition of $x = 0.62$ and a tensile strain of 0.1% corresponding to multicritical point at the boundary between 5 polydomain phases. Large pyroelectric coefficients exceeding 0.03 μC/cm^{2}K in magnitude can also be obtained at the boundary between the *c/a/c/a* and the $a_1/a_2/a_1/a_2$ phases over a wide range of composition. This reveals the complexity of predicting the optimum value of pyroelectric coefficient in such systems and suggests that neither proximity to T_c nor the magnitude of polarization alone provide enough information to completely maximize π. In reality, other factors

such as strain driven polarization transitions and the susceptibility of domain walls to temperature can greatly impact the properties of these materials and in turn, dominate responses in epitaxial thin films. In fact, as shown in Fig. 2, the domain wall effects can dominate the intrinsic response and one needs to take into account domain wall displacements to completely understand and estimate the properties of ferroelectric films. Again, to recap, we observe that the pyroelectric coefficient is increased for mild tensile strains ($S_m < 0.5\%$) and is, on average, larger for Ti-rich films.

We note that this calculation assumes that the domain walls are free to move without any energy barriers. In reality lattice imperfections or defects can pin domain walls, hinder their movement, and reduce the extrinsic contribution. The extrinsic contribution to pyroelectric response will be zero in the case of completely pinned domain walls and our calculation, in effect, places an upper bound on the extrinsic contribution to the pyroelectric properties. The energy barriers for the 90° domains considered here are much smaller than the 180° domain walls[33] and the 90° domain walls are expected to move quite freely at $T \geq 300$ K in epitaxial thin films. Since the extrinsic contribution reduces the total pyroelectric coefficient for compressively strained films, one could also increase the pyroelectric coefficient for compressively strained films using some form of nanoscale domain wall pinning (possible through focused ion-beam (FIB) patterning of defects) or lowering the temperature, thereby rendering the domain walls immobile. Similarly, any form of domain pinning will serve to reduce the pyroelectric coefficients in tensile strained films.

Thus far we have focused only on the primary pyroelectric coefficient in materials and have excluded secondary contributions. In a real system, temperature dependent changes in crystal shape will result in piezoelectric contributions to the pyroelectric response. The model

thus far, has considered the substrate to be a passive medium that influences the pyroelectric properties of the film through the epitaxial strain alone; however, the difference in thermal expansion between the substrate and the ferroelectric thin film can also influence the pyroelectric properties. Again, this contribution is referred to as the secondary pyroelectric coefficient (π_s) and has generally been neglected since early estimates suggested that it should be considerably smaller than the primary effect in epitaxial thin films that are clamped in-plane to a thick substrate.[34] These early studies provided only a preliminary discussion on the secondary effect in epitaxial thin films and thus we expand this here to provide a more rigorous calculation for the case of PZT thin films. This will enable a deeper understanding of pyroelectricity in thin films and will provide insight into situations that might call for inclusion of this effect in calculations of pyroelectric coefficients. For an epitaxially clamped thin film, the secondary pyroelectric coefficient can be calculated as[34]

$$\pi_s = -\frac{2d_{31}^f\left(\alpha^f - \alpha^s\right)}{s_{11}^f + s_{12}^f} \tag{6}$$

where d_{31}^f is the piezoelectric coefficient of the thin film and s_{ij}^f are the elements of the elastic compliance tensor for the thin film. α^f and α^s are the thermal expansion coefficients of the film and the substrate, respectively. The piezoelectric coefficient d_{31}^f is related to the bulk value d_{31}^B by[35]

$$d_{31}^f = d_{31}^B \frac{s_{11}^s + s_{12}^s}{s_{11}^f + s_{12}^f} \tag{7}$$

where s_{ij}^s are the elastic compliance coefficients of the substrate. Thus, we can write the total secondary component of the pyroelectric coefficient (π_s) for epitaxial thin films as

$$\pi_s = -\frac{2d_{31}^B(s_{11}^s + s_{12}^s)(\alpha_f - \alpha_s)}{(s_{11}^f + s_{12}^f)^2} \tag{8}.$$

We immediately see that the secondary pyroelectric coefficient depends on the thermal and mechanical properties of the substrate and an estimation of this contribution requires intimate knowledge of the substrate that is used to impart the strain. This is in stark contrast to the primary pyroelectric coefficient which depends only on the ferroelectric material. Among the standard single crystal oxide substrates that are used to for epitaxial growth of PZT thin films across the strain regime we have investigated herein ($-0.02 \leq S_m \leq 0.02$), the thermal expansion coefficients and elastic constants are available only for two: $SrTiO_3$ (STO)[36,37,38] and $GdScO_3$ (GSO).[39,40] We focus here on the analysis of films grown on these two substrates to estimate the secondary pyroelectric coefficient for PZT thin films as a function of composition. The thermal expansion coefficient, elastic constants, and piezoelectric coefficients for PZT were obtained from Refs. 29, 37, 41, and 42. The various values of these coefficients used in this analysis are provided in Table I. Fig. 5(a) shows the variation of the secondary pyroelectric coefficient as a function of Ti content for a PZT film grown on both a STO and GSO substrate. The secondary contribution is found to increase dramatically near the morphotropic phase boundary in PZT, but remains small and relatively constant for high Ti-concentrations. From this analysis, we see that the secondary contribution is larger for PZT films on STO substrates, thus we have gone on to calculate all contributions to the pyroelectric coefficient (intrinsic, extrinsic, and secondary) to provide a complete analysis for a model thin film heterostructure [Fig. 5(b)]. From this work, it is clear that the secondary pyroelectric coefficient is generally smaller than the intrinsic contribution, is always negative, and has a maximum value near the morphotropic phase boundary ($x \sim 0.5$) where the piezoelectric coefficient d_{31} attains a maximum value. Therefore, the secondary pyroelectric coefficient adds or enhances the primary effect and the relative importance of this effect is exacerbated as one approaches the morphotropic phase boundary.

Thus, the exclusion of the secondary effect provides us with a conservative estimate of the maximum pyroelectric coefficient that can be attained in these thin films.

The extrinsic effect, on the other hand, can dramatically change the nature of the total pyroelectric coefficient as demonstrated [Fig. 5(b)]. Thus when attempting to analyze a large phase space in materials (i.e., the large strain and composition space undertaken here), it is reasonable to focus on the primary (intrinsic and extrinsic) pyroelectric effect to provide a strong foundation for the physics of the materials. At such coarse levels and acknowledging that the secondary effect is small in magnitude, it is reasonable to exclude this effect during initial investigations. Once research is focused on a specific film-substrate system, however, addition of the secondary effect will provide a more complete picture and accurate prediction of pyroelectric coefficients in such systems. It is clear that additional experimental determinations of the thermal expansion coefficients and elastic constants for common oxide substrates will be a boon for further theoretical studies. Such a detailed analysis of pyroelectric effects in materials has not been addressed in earlier work and we hope that our study enables the fabrication improved ferroelectric thin films for various pyroelectric applications and prompts further study of properties in these oxide materials.

IV. CONCLUSIONS

We have developed a model of pyroelectric effects in materials that takes into account intrinsic, extrinsic, and secondary contributions to response. Our thermodynamic calculations show that extrinsic contributions to the pyroelectric coefficient due to temperature induced domain wall displacements can be very influential in ferroelectric thin films and provides a theoretical platform to systematically optimize the performance of pyroelectric thin films as a function of strain, temperature, and composition. We show that extrinsic contributions can

greatly enhance the pyroelectric coefficient in tensile strained films. Large pyroelectric coefficients were observed along the boundary between the $c/a/c/a$ and the $a_1/a_2/a_1/a_2$ phases and at the critical point between the various polydomain phases. Further, for room temperature applications, high Ti content and tensile strains were observed to give rise to large pyroelectric response. Additionally, we have investigated the secondary pyroelectric effect, which has generally been neglected in thin film calculations, which has been shown to be small in magnitude as compared to the primary contribution and directly dependent on the substrate that is used. In general this secondary contribution increases the magnitude of the total pyroelectric coefficient of PZT thin films, because important in materials near the morphotropic phase boundary, and provides a fine-adjustment and more accurate prediction of pyroelectric properties in thin film systems.

In the past, the pyroelectric performance of thin films has been observed to generally be inferior to bulk crystals,[17,18] but large pyroelectric coefficients have been observed[32,43] in select thin films systems. Our study provides a physical understanding of the pyroelectric effect in polydomain films and helps gain a deeper insight towards rationalizing the observed pyroelectric properties of thin films. We hope that this new insight will initiate further studies into other novel domain wall driven phenomena and help synthesize high performance thin films that find widespread practical applications. The need for high performance pyroelectric materials will continue to grow in the coming years and with this we need to develop routes to maximize the effects in existing materials and systems. The current approach demonstrates a simple design methodology that allows for the optimization of pyroelectric response in polydomain ferroelectric thin films. In order to appropriately optimize the material response, one must

balance the competing factors and carefully inspect the system at hand in order to choose the right synthesis parameters like strain, substrate and composition.

ACKNOWLEDGMENTS

The authors acknowledge support from the Office of Naval Research under Grant Number N00014-10-10525.

References

[1] B. Jaffe, W.R. Cook, and H. Jaffe*, Piezoelectric Ceramics* (Academic, London, 1971).

[2] M. Dawber, K. M. Rabe, J. F. Scott, Rev. Mod. Phys. 77, 1083 (2005).

[3] N. Setter, D. Damjanovic, L. Eng, G. Fox, S. Gevorgian, S. Hong, A. Kingon, H. Kohlstedt, N. Y. Park, G. B. Stephenson, I. Stolitchnov, A. K. Taganstev, D. V. Taylor, T. Yamada, and S. Streiffer, J. Appl. Phys. **100**, 051606 (2006).

[4] D. G. Schlom, L. Q. Chen, C. B. Eom, K. M. Rabe, S. K. Streiffer, and Jean-Marc Triscone, Annu. Rev. Mater. Res. **37** 589 (2007).

[5] V. Nagarajan, S. Prasertchoung, T. Zhao, H. Zheng, J. Ouyang, R. Ramesh, W. Tian, X. Q. Pan, D. M. Kim, C. B. Eom, H. Kohlstedt, and R. Waser, Appl. Phys. Lett. **84**, 5225 (2004)

[6] Y. L. Li, S. Y. Hu, Z. K. Liu, and L. Q. Chen, Appl. Phys. Lett. **81**, 427 (2002).

[7] J. H. Haeni, P. Irvin, W. Chang, R. Uecker, P. Reiche, Y. L. Li, S. Choudhury, W. Tian, M. E. Hawley, B. Craigo, A. K. Tagantsev, X. Q. Pan, S. K. Streiffer, L. Q. Chen, S. W. Kirchoefer, J. Levy and D. G. Schlom, Nature **430**, 758 (2004).

[8] G. Catalan, A. Janssens, G. Rispens, S. Csiszar, O. Seeck, G. Rijnders, D. H. A. Blank, and B. Noheda, Phys. Rev. Lett. **96**, 127602 (2006).

[9] R. J. Zeches, M. D. Rossell, J. X. Zhang, A. J. Hatt, Q. He, C.-H. Yang, A. Kumar, C. H. Wang, A. Melville, C. Adamo, G. Sheng, Y.-H. Chu, J. F. Ihlefeld, R. Erni, C. Ederer, V. Gopalan, L. Q. Chen, D. G. Schlom, N. A. Spaldin, L. W. Martin and R. Ramesh, Science **326**, 977 (2009).

[10] P. Muralt, Rep. Prog. Phys. **64** 1339 (2001).

[11] R. Bruchhaus, D. Pitzer, M. Schreiter and W. Wersing, Journal of Electroceramics **3**, 151 (1999).

[12] M. E. Lines and A. M. Glass, *Principles and Applications of Ferroelectrics and Related Materials* (Oxford University Press, New York, 1979).

[13] R. W. Whatmore, Rep. Prog. Phys. **49**, 1335 (1986).

[14] R. B. Olsen, D. A. Bruno, and J. M. Briscoe, J. Appl. Phys. **58**, 4709 (1985).

[15] G. Sebald, S. Pruvost, and D. Guyomar, Smart Mater. Struct. **17**, 015012 (2008).

[16] A. N. Morozovska, E. A. Eliseev, G. S. Svechnikov, and S. V. Kalinin, J. Appl. Phys. **108**, 042009 (2010).

[17] A. Sharma, Z. G. Ban, S. P. Alpay, and J. V. Mantese, J. Appl. Phys. **95**, 3618 (2004).

[18] Z. G. Ban and S. P. Alpay, Appl. Phys. Lett. **82**, 3499 (2003).

[19] A. H. G. Vlooswijk, B. Noheda, G. Catalan, A. Janssens, B. Barcones, G. Rijnders, D. H. A. Blank, S. Venkatesan, B. Kooi, and J. T. M. de Hosson, Appl. Phys. Lett. **91**, 112901 (2007).

[20] Q. Y. Qiu, S. P. Alpay, and V. Nagarajan, J. Appl. Phys. **107**, 114105 (2010).

[21] J. S. Speck, A. Seifert, W. Pompe, and R. Ramesh, J. Appl. Phys. **76**, 477 (1994).

[22] S. P. Alpay, V. Nagarajan, L. A. Bendersky, M. D. Vaudin, S. Aggarwal, R. Ramesh, and A. L. Roytburd, J. Appl. Phys. **85**, 3271 (1999).

[23] V. G. Koukhar, N. A. Pertsev, and R. Waser, Phys. Rev. B **64**, 214103 (2001).

[24] V. G. Kukhar, N. A. Pertsev, H. Kohlstedt, and R. Waser, Phys. Rev. B **73**, 214103 (2006).

[25] C. S. Ganpule, V. Nagarajan, B. K. Hill, A. L. Roytburd, E. D. Williams, R. Ramesh, S. P. Alpay, A. Roelofs, R. Waser, and L. M. Eng, J. Appl. Phys. **91**, 1477 (2002).

[26] N. A. Pertsev and A. G. Zembilgotov, J. Appl. Phys. **78**, 6170 (1995).

[27] N. A. Pertsev and A. G. Zembilgotov, J. Appl. Phys. **80**, 6401 (1996).

[28] M. J. Haun, Z. Q. Zhuang, E. Furman, S. J. Jang, and L. E. Cross, Ferroelectrics **99**, 45 (1989).

[29] L.-Q. Chen, *Landau Free-Energy Coefficients, Physics of Ferroelectrics: A Modern Perspective* (Springer-Verlag, Berlin, 2007).

[30] N. A. Pertsev, V. G. Kukhar, H. Kohlstedt, and R. Waser, Phys. Rev. B **67**, 054107 (2003).

[31] Y. Watanabe, Phys. Rev. B **57**, 789 (1998).

[32] Y. Ivry, V. Lyahovitskaya, I. Zon, I. Lubomirsky, E. Wachtel, and A. L. Roytburd, Appl. Phys. Lett. **90**, 172905 (2007).

[33] B. Meyer and D. Vanderbilt, Phys. Rev. B **65**, 104111 (2002).

[34] J. D. Zook and S. T. Liu, J. Appl. Phys. **49**, 4604 (1978).

[35] Jun Ouyang, Ph.D. Thesis, University of Maryland, College Park (2005).

[36] A. L. Roytburd, S. P. Alpay, L. A. Bendersky, V. Nagarajan, R. Ramesh, J. Appl. Phys. **89**, 553 (2001).

[37] H. Nakaki, Y. K. Kim, S. Yokoyama, R. Ikariyama, H. Funakubo, K. Nishida, K. Saito, H. Morioka, O. Sakata, H. Han, S. Baik, J. Appl. Phys. **105**, 014107 (2009).

[38] Numerical Data and Functional Relationships in Science and Technology, Landolt-Bornstein New Series Vol. III/29a edited by K. H. Hellwege and A. M. Hellwege (Springer, New York, 1981).

[39] M. D. Biegalski, J. H. Haeni, S Troiler-McKinstry, D. G. Schlom, C. D. Brandle. A. J. V. Graitis, J. Mater. Res. **20,** 952 (2005).

[40] K. A. Petska, J. D. Maynard, A. Soukiassian, X. X. Xi, D. G. Schlom, Y. Le Page, M. Bernhagen, P. Reiche and R. Uecker, Appl. Phys. Lett. **92**, 111915 (2008).

[41] G. H. Haertling, J. Amer. Ceram. Soc. **54**, 303 (1971).

[42] M. J. Haun, E. Furman, S. J. Jang and L. E. Cross, Ferroelectrics **99**, 63 (1989).

[43] F. Jin, G. W. Auner, R. Naik, N. W. Schubring, J. V. Mantese, A. B. Catalan, and A. L. Micheli, Appl. Phys. Lett. **73**, 2838 (1998).

Figures Captions

Fig. 1. Strain – composition phase diagram of $PbZr_{1-x}Ti_xO_3$ thin films showing the polarization pattern in the various equilibrium polydomain states along with illustrations of the domain configurations.

Fig. 2. Dependence of the pyroelectric coefficient with epitaxial strain for $PbZr_{1-x}Ti_xO_3$ thin films with x = (a) 1.0, (b) 0.9, (c) 0.8, (d) 0.7, (e) 0.6, and (f) 0.5. The red line indicates the total pyroelectric coefficient (intrinsic + extrinsic) while the blue line shows the pyroelectric coefficient assuming pinned domain walls, i.e. zero extrinsic contribution.

Fig. 3. Effect of strain on the extrinsic contribution to pyroelectric coefficient in the polydomain *c/a/c/a* phase. With an increase in temperature, the equilibrium fraction of the c phase (f_c) increases for compressive strains and decreases for tensile strains. The spontaneous polarization within the domains (P_s) however, decreases with increases in temperature for all values of strain.

Fig. 4. Strain – composition phase diagram of $PbZr_{1-x}Ti_xO_3$ thin films showing the pyroelectric coefficient at 300 K for the various equilibrium polydomain states.

Fig. 5. (a) Dependence of the secondary pyroelectric coefficient with Ti content for $PbZr_{1-x}Ti_xO_3$ thin films on two substrates: $SrTiO_3$ (blue) and $GdScO_3$ (orange). (b) Intrinsic (orange), extrinsic (red), secondary (blue), and total (black) pyroelectric coefficients for $PbZr_{1-x}Ti_xO_3/SrTiO_3$ thin film.

Table I. Thermal expansion coefficient and elastic constants for a range of $PbZr_{1-x}Ti_xO_3$ materials and substrates.

Material	Thermal Expansion Coeff. (α, K^{-1})	Elastic Constants (x 10^{-12} m^2/N)	
		s_{11}	s_{12}
$PbZr_{0.5}Ti_{0.5}O_3$	5.4 x 10^{-6}	10.5	-3.7
$PbZr_{0.4}Ti_{0.6}O_3$		8.6	-2.8
$PbZr_{0.3}Ti_{0.7}O_3$		8.4	-2.7
$PbZr_{0.2}Ti_{0.8}O_3$		8.2	-2.6
$PbZr_{0.1}Ti_{0.9}O_3$		8.1	-2.5
$PbTiO_3$		8.0	-2.5
$SrTiO_3$	11.1 x 10^{-6}	3.75	-0.92
$GdScO_3$	10.9 x 10^{-6}	3.97	-1.98

Table 1 BB11447 04MAY2011

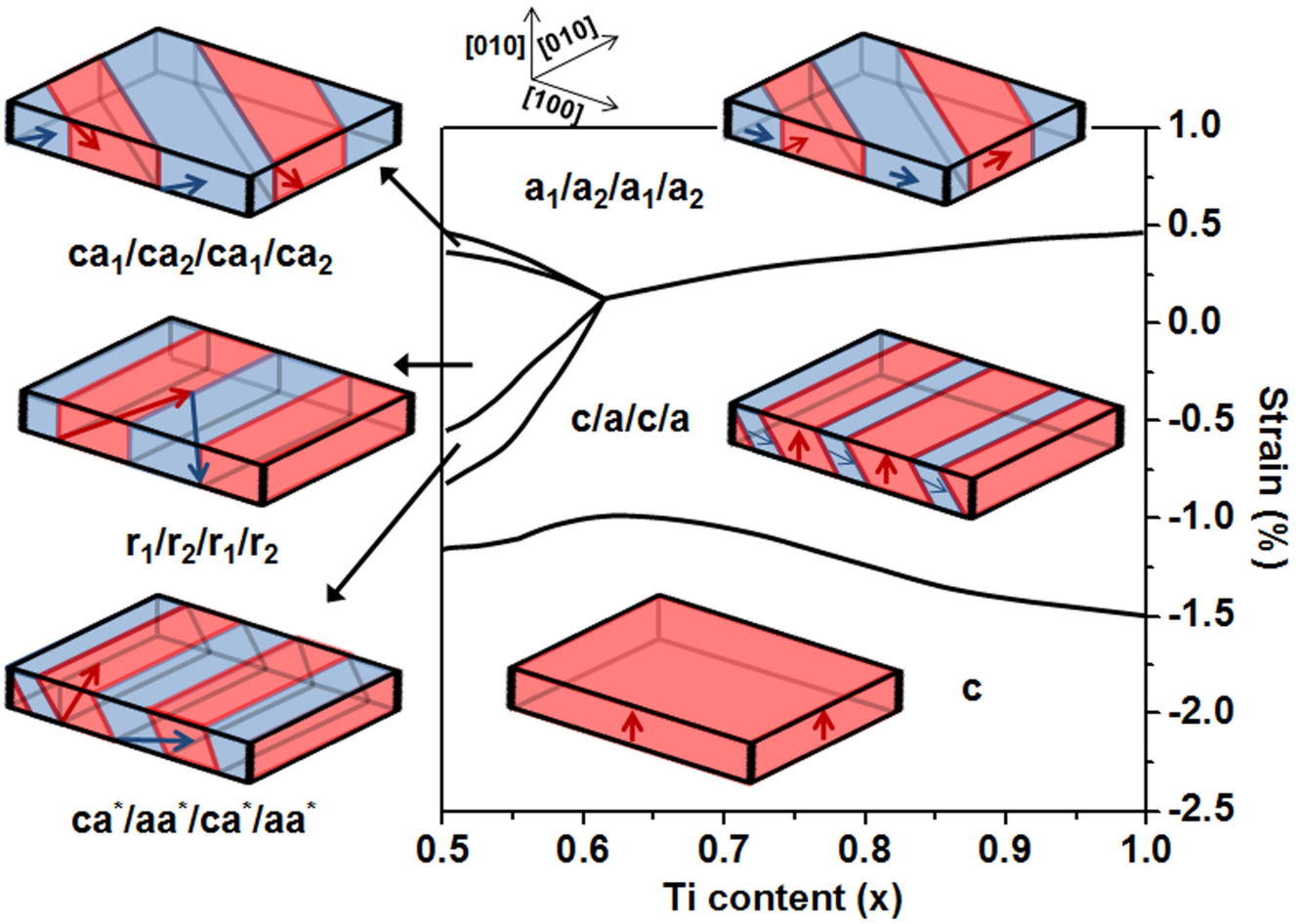

Figure 1 BB11447 04MAY2011

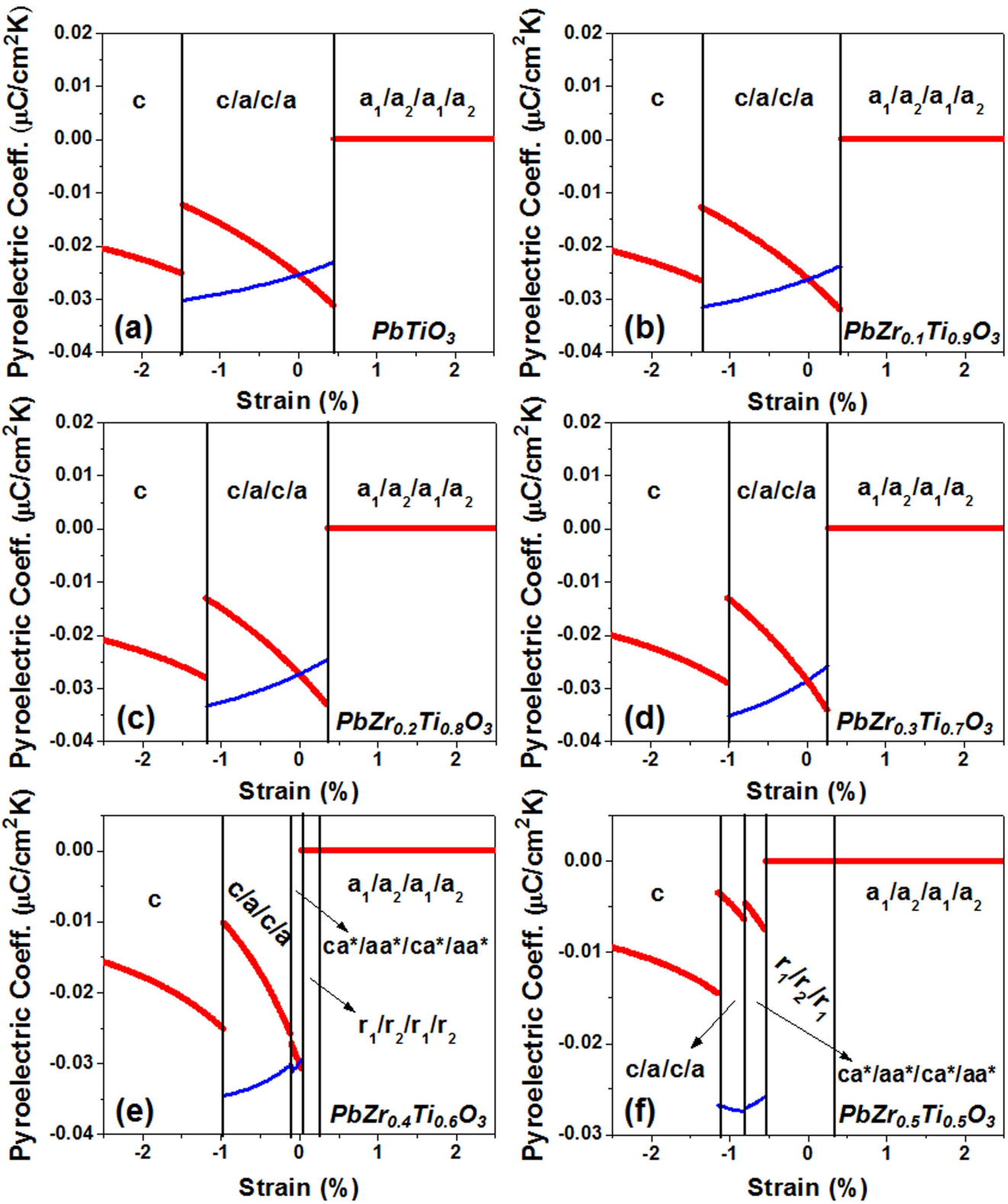

Figure 2 BB11447 04MAY2011

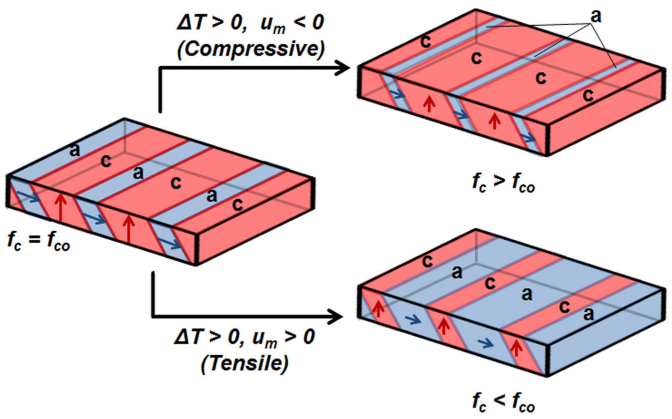

Figure 3 BB11447 04MAY2011

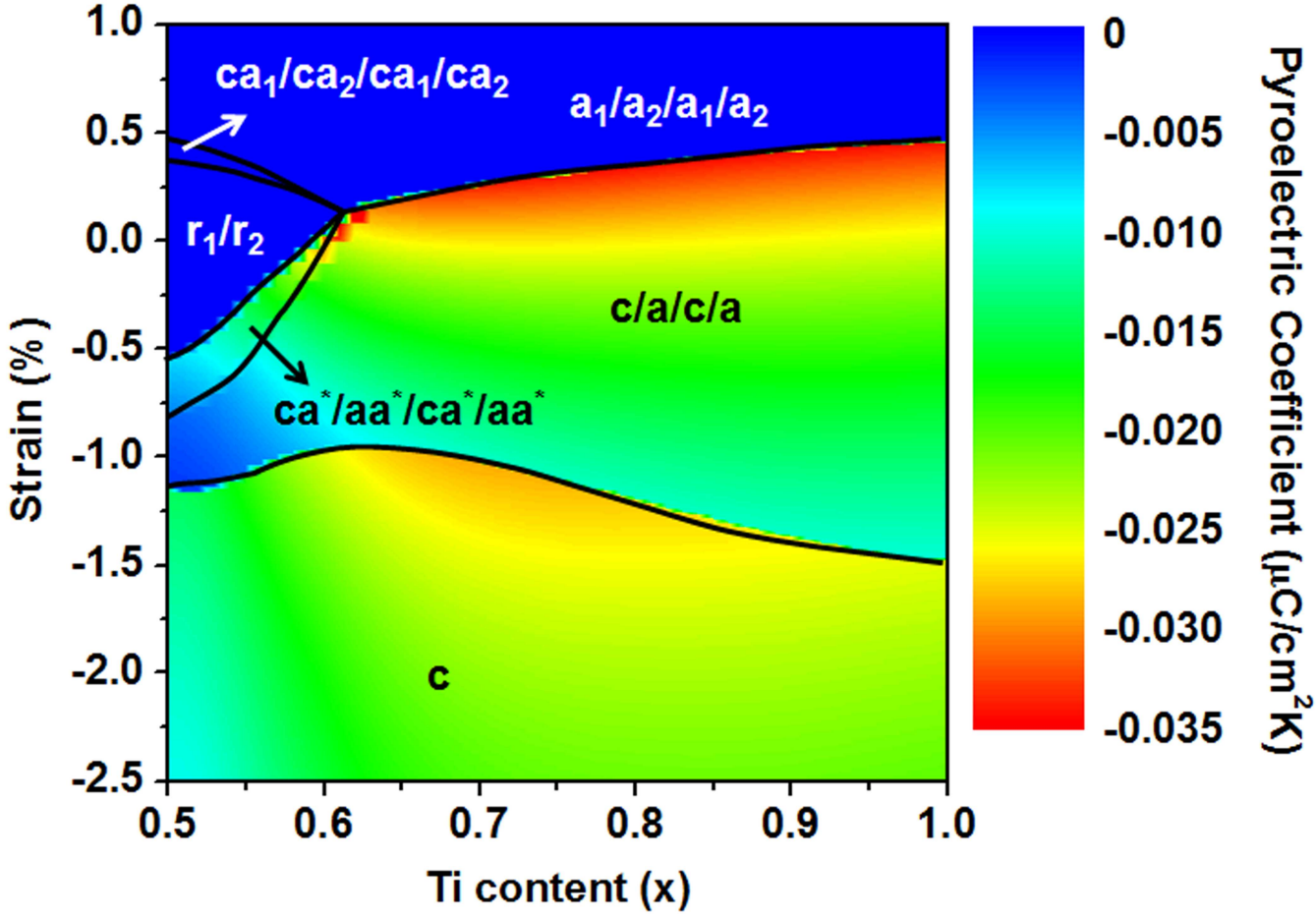

Figure 4 BB11447 04MAY2011

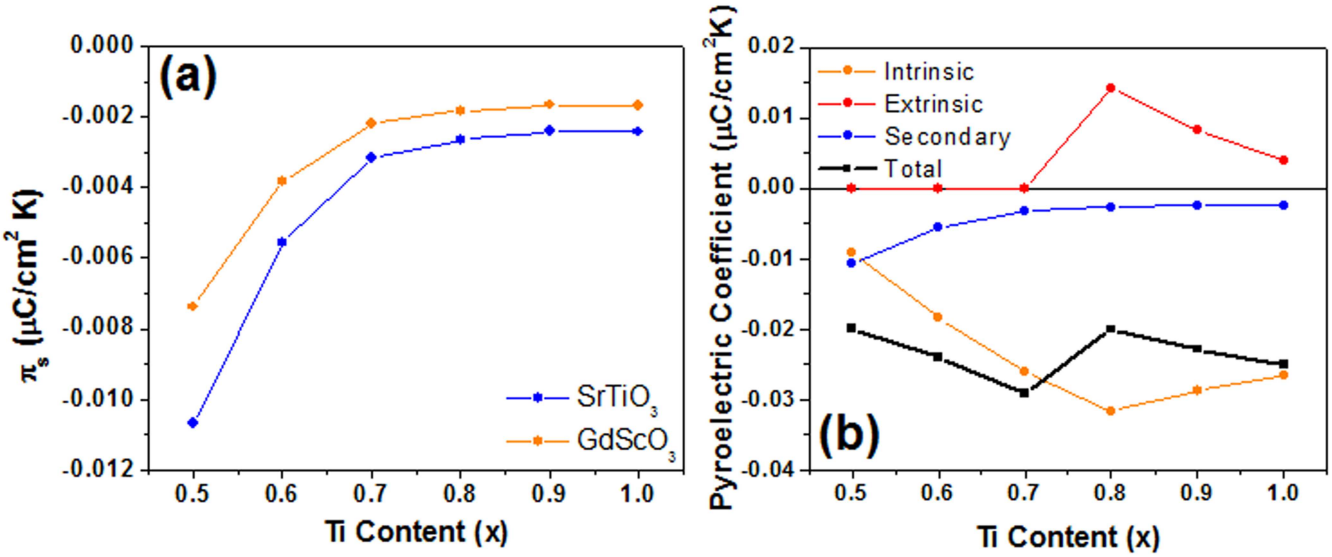

Figure 5 BB11447 04MAY2011